

LED: Light Enhanced Depth Estimation at Night

Simon de Moreau^{1,2}Yasser Almeheio²Andrei Bursuc³Hafid El-Idrissi²Bogdan Stanciulescu¹Fabien Moutarde¹

Abstract

Nighttime camera-based depth estimation is a highly challenging task, especially for autonomous driving applications, where accurate depth perception is essential for ensuring safe navigation. We aim to improve the reliability of perception systems at night time, where models trained on daytime data often fail in the absence of precise but costly LiDAR sensors. In this work, we introduce Light Enhanced Depth (LED), a novel cost-effective approach that significantly improves depth estimation in low-light environments by harnessing a pattern projected by high definition headlights available in modern vehicles. LED leads to significant performance boosts across multiple depth-estimation architectures (encoder-decoder, Adabins, DepthFormer) both on synthetic and real datasets. Furthermore, increased performances beyond illuminated areas reveal a holistic enhancement in scene understanding. Finally, we release the Nighttime Synthetic Drive Dataset, a new synthetic and photo-realistic nighttime dataset, which comprises 49,990 comprehensively annotated images. To facilitate further research, both synthetic dataset and code are publicly available at <https://simondemoreau.github.io/LED/>.

1. Introduction

Adverse conditions, such as harsh weather or nighttime, pose significant challenges to many computer vision applications. Despite impressive progress in perception systems for autonomous driving, enabled by powerful deep neural architectures and training techniques, the challenges of nighttime navigation persist, demanding precise scene comprehension. Accurate depth estimation is a crucial aspect of perception and extends beyond immediate applications, profoundly impacting overall scene perception, especially at night [37]. While LiDAR sensors offer high accuracy, their widespread adoption is impeded by substantial costs.

Additionally, in humid weather such as fog or rain, LiDAR effectiveness can be significantly degraded due to beam reflection and increased noise levels [6, 7].

Cameras are powerful and cost-effective sensors capturing rich information about the environment while deployed in most modern-day vehicles. Camera-based perception solutions displays high reliability and accuracy [1, 4, 5, 15–17, 23], but mostly on clear daylight conditions. However, they struggle under distribution shift and low-light conditions. An additional challenge is related to the availability of labeled data for training high-capacity deep neural networks. For the task of depth estimation, some methods rely on supervised learning [1, 4, 20, 23], most use self-supervised methods [5, 16, 17, 32, 36, 45–48] since obtaining dense ground truth depth information can be expensive. While dedicated approaches for particular conditions arised in the past few years [24, 38, 40, 45, 47] they are still partially mitigating these issues. To the best of our knowledge, they remain limited to self-supervised strategies due to the absence of publicly available large-scale annotated datasets suitable for nighttime depth estimation training. This paper introduces a new annotated nighttime synthetic dataset featuring dense depth maps, among other labels.

To improve the performance of supervised methods in low-light conditions, we draw inspiration from active stereovision methods [2, 13, 21, 33] by harnessing High-Definition (HD) headlights commonly equipped in modern vehicles. These headlights have demonstrated promising results in scene perception research [41–43]. Therefore, we leverage them to project a pattern into the scene, guiding the network and thereby improving perception accuracy and reliability.

In this paper, we introduce Light Enhanced Depth (LED), a novel approach that significantly improves depth estimation in low-light environments, ensuring enhanced accuracy and robust performances for autonomous vehicles. Our contributions can be summarized as follows:

- **Enhanced Depth Estimation:** Using only an encoder-decoder as depth-estimation model, we demonstrate a remarkable -11% RMSE improvement at nighttime by incorporating HD headlight pattern.
- **Architecture-Agnostic:** We extend our methodology

¹Center for Robotics - Mines Paris - PSL University, France, {simon.de.moreau, bogdan.stanciulescu, fabien.moutarde}@minesparis.psl.eu

²Valeo, France, {simon.de-moreau, yasser.almeheio, hafid.el-idrissi}@valeo.com

³Valeo.ai, France, andrei.bursuc@valeo.com

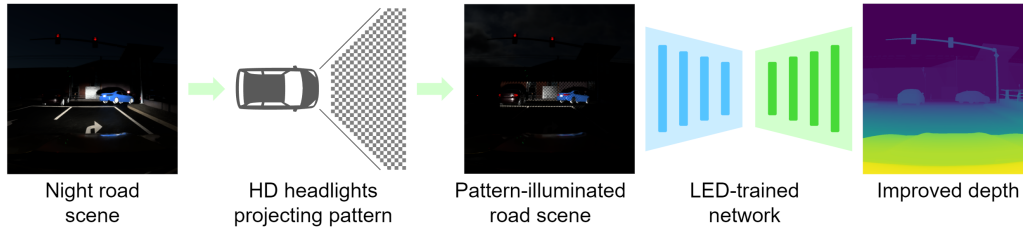


Figure 1. LED (Light Enhanced Depth) is a novel method enhancing depth estimation from nighttime RGB images by harnessing High-Definition headlights’ pattern. We release a new synthetic nighttime dataset containing both high beam and pattern-illuminated RGB images, associated with comprehensive ground truth annotations. This dataset will facilitate research into nighttime perception across various applications.

to two other state-of-the-art (SOTA) methods designed for daytime scenarios, showcasing its versatility and performance improvement across diverse neural network architectures (-24.06% RMSE on Adabins [4], -8.00% RMSE on DepthFormer [23]).

- **Global Scene Understanding:** We show that our proposed method enhances the overall understanding of the scene beyond illuminated area with -3.05% RMSE on the whole image.
- **Dataset:** We provide the Nighttime Synthetic Drive Dataset, a photorealistic synthetic dataset comprising 49,995 comprehensively annotated nighttime images to foster future investigations in nighttime perception.
- **Real prototype:** LED also demonstrates great performances improvements on our in-house dataset, collected using a real car-mounted prototype.

2. Related Work

2.1. Daytime Depth Estimation Methods at Night

Supervised Learning from Monocular Camera. Recent advances in supervised depth prediction exploit transformer architectures and attention mechanisms [1, 4, 20, 23] to improve performances. These methods highlight the effectiveness of transformer-based architectures and the strategic use of bins [1, 4] in improving depth prediction accuracy, even with more limited datasets available [9, 14, 27, 29] compared to self-supervised methods [5, 16, 17, 32, 36, 46, 48].

However, to the best of our knowledge, these methods are confined to daytime scenarios. Nighttime depth estimation approaches [45, 47] currently rely on self-supervised methods. This limitation stems from the scarcity of large-scale nighttime datasets and, even more so, the lack of properly annotated ones. In response, we release the Nighttime Synthetic Drive Dataset, to support the development of approaches adapted to nighttime scenarios.

Nighttime Domain Adaptation. [40] and [38] tackle nighttime depth estimation as a domain adaptation challenge, focusing on common feature representations for daytime and

nighttime images. The former maintains performance by aligning night image encoder features with pre-trained daytime encoder features. Similarly, the latter enhances nighttime depth estimation by leveraging dense features representation across domains. In contrast, [24] reject the assumption of identical features in both domains. To capture their nuances, they train independent feature extractors with losses considering domains similarities and differences. With LED, we tailor our method to fit the unique features of nighttime scenes by leveraging the informative deformations of the light pattern emitted by a vehicle’s HD headlamp.

2.2. Specific Modalities for Nighttime

LiDAR or thermal imaging [26, 35] can be used to overcome low-light challenges. However, these approaches require paired data for training and entail extra expenses for sensors and computational power needed for vehicle integration. In this work, we address nighttime challenges by leveraging built-in equipment available in modern vehicles.

2.3. Light for Perception

Active Stereo vision. Depth estimation based on active stereo vision involves disparity measurement. Unlike traditional stereo vision, disparity is computed between an image and a pattern projected onto the scene. Recent methods [2, 13, 21, 33] use deep learning models designed to take patterns and images as input. They propose specific loss functions dedicated to disparity maps.

While active stereo vision offers valuable scale information, it has demonstrated significant performance degradation when deployed outdoors, due to high ambient lighting and the low power of projectors [8, 18, 28]. We avoid this degradation thanks to our nighttime environment characterized by low illumination conditions and the utilization of high-powered visible HD headlights, resulting in favorable conditions for our approach.

HD Lighting. HD lighting has been a research interest for years, but its recent industrialization explains the limited number of related works. A series of articles [11, 39]

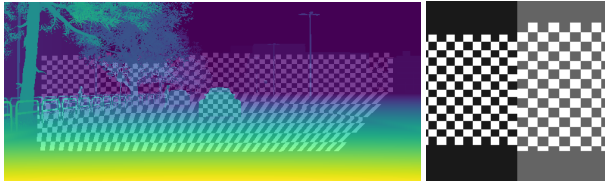


Figure 2. Pattern deformation and size variation in the scene: left image shows the pattern projection on a depth image, computed using geometrical rules. It demonstrates trapezoidal deformations on horizontal surfaces and undistorted squares on vertical surfaces. Complex deformations on the car reveal insights into its geometry. The right image showcases the pattern size projected on a wall at 10 m (darker background) and 100 m (lighter background). Note that square sizes increase with distance.

highlight its potential applications and particularly its ability to design anti-glare systems while optimizing illumination for enhanced driver visibility. They have also demonstrated improved driver visibility in adverse conditions such as rain or snow. More recently, [44] proposed reducing overall scene illumination to decrease power consumption while maintaining object detection capabilities. To facilitate these experiments, the same team has proposed hardware-in-the-loop simulation solutions for headlights [41–43].

We introduce a novel application of HD headlights to improve understanding of overall scene geometry and enhance depth estimation. We achieve this by projecting a pattern onto the nighttime scene, providing guidance for the model.

3. Method

We improve depth estimation from monocular camera at nighttime by leveraging a pattern projected in front of the vehicle with HD headlights.

3.1. HD Pattern and Headlights

Networks designed for active stereovision exploit the disparity between the projected pattern and the camera’s view to estimate distances within the scene. In LED, a model identifies pattern’s areas that deviate from the implicitly learned reference pattern.

Diverging from traditional active stereovision which relies on infrared lasers projecting points, we harness an HD headlight. Similar to a beamer, this type of headlight can dynamically project any image or shape onto the scene. Specifically, we simulate a real 3,696 pixels HD headlight (132×28 px) with a horizontal Field of View (FOV) of 35° and a vertical FOV of 7° . The emitted light is not colimated, thus, similar to a projector, the size of a pixel in the projection varies with distance. We illustrate it in Fig. 2, as the projection extends further, a pixel appears larger. This provides the neural network with valuable cues about distances in the scene. To avoid superposition of HD patterns we only use the left headlight.

We employ a regular checkerboard pattern because of its ability to exhibit high discontinuities and strong contrast. The dense concentration of corners and transitions in the pattern serves as features easily recognizable and detectable by convolutional neural networks [3]. These features aid the network in extracting the pattern from the scene. Dimensions of the checkerboard cells are 0.5° , ensuring proper visibility with the simulated camera resolution.

Upon projection, the checkerboard undergoes deformations (from the camera’s perspective) based on surface’s shape. As illustrated in Fig. 2, horizontal planes tend to stretch the pattern into a trapezoid, while vertical surfaces parallel to image plane do not cause any deformation. More complex deformations occur on non-planar surfaces such as cars. All these elements provide valuable information about the scene’s geometry to the network and thus enhances the quality of depth estimation.

3.2. Architectures

Our method is architecture-agnostic. Since we rely on a single pattern, the model can learn the reference pattern implicitly. Consequently, there is no need to design a dedicated network architecture to handle it.

To showcase the benefits of using a projected HD pattern for depth estimation, we employ an encoder-decoder model (U-Net [34]) for most of our studies. This model takes a single RGB image with the projected pattern as input and estimates depth map as output. Despite the simplicity of this architecture, it achieve results on par with or superior to other SOTA methods (see Sec. 5.1).

We successfully apply our method to more complex SOTA architectures: DepthFormer [23] and Adabins [4], with similar performances enhancement (see Sec. 5.4).

3.3. Learning Objectives

To train the encoder-decoder, we adopt a combination of loss functions inspired by [19]. The primary loss, \mathcal{L}_{depth} , is the Log L1 loss presented in Eq. (1). It measures the error between the estimated depth, d_i , and the corresponding ground truth, g_i . This variant of L1 loss attributes less significance to errors occurring at greater distances. This adjustment aligns with the expectation that given errors, e.g. 1 m, should have greater impact when within a few meters of the camera but are more tolerable at extended distances.

$$\mathcal{L}_{depth} = \frac{1}{N} \sum_{i=1}^N |\log(d_i) - \log(g_i)| \quad (1)$$

We address edges fidelity, particularly challenging in low-light conditions. To this end, we incorporate a loss, \mathcal{L}_{grad} , that specifically emphasizes on gradients. As we believe edges sharpness is important regardless of the distance, we employ a standard L1 Loss expressed in Eq. (2)

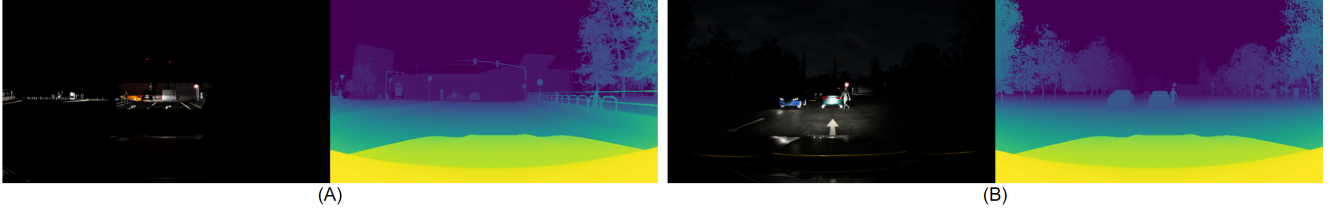


Figure 3. Nighttime Synthetic Drive Dataset examples: (A) depicts HD pattern and (B) high-beam illumination. Ground truth annotations include dense depth maps, semantic segmentation, instance segmentation labels and bounding boxes.

instead of a logarithmic one used in [19]. Moreover, our experiments revealed no performance improvements with the Log version. $\nabla_x(d_i)$ and $\nabla_y(d_i)$ respectively represent the spatial derivative of d_i along the x and y-axis.

$$\mathcal{L}_{grad} = \frac{1}{N} \sum_{i=1}^N |\nabla_x(d_i) - \nabla_x(g_i)| + |\nabla_y(d_i) - \nabla_y(g_i)| \quad (2)$$

Similar to [19], we want to ensure accurate surfaces representation in depth maps. The depth normals are estimated at each pixel using $n_i^a \equiv [-\nabla_x(a_i), -\nabla_y(a_i), 1]^T$. The cosine similarity loss, expressed in Eq. (3), is then employed to compare estimated and ground truth normals. $\langle \cdot, \cdot \rangle$ denotes vector inner product operation.

$$\mathcal{L}_{normal} = \frac{1}{N} \sum_{i=1}^N \left| 1 - \frac{\langle n_i^d, n_i^g \rangle}{\sqrt{n_i^d} \sqrt{n_i^g}} \right| \quad (3)$$

Finally, our learning objective can be expressed as Eq. (4), we set $\lambda_1 = 1$ and $\lambda_2 = 1$.

$$\mathcal{L} = \mathcal{L}_{depth} + \lambda_1 \mathcal{L}_{grad} + \lambda_2 \mathcal{L}_{normal} \quad (4)$$

3.4. Implementation Details

We implement the encoder-decoder in PyTorch [31]. For each experiment the model is trained from scratch during 70 epochs using the AdamW optimizer [25]. The training is conducted with a batch size of 32, and both input and output resolutions are set to 320×320 px. The learning rate is set to 10^{-3} and the selection of the best epoch is based on the Root Mean Square Error (RMSE) metric. This determination is made on a 5,000 images validation set. The entire training process takes approximately 4 hours, conducted on a single Nvidia RTX 4090.

Adabins was implemented using the official code from [4], while we rely on the Monocular-Depth-Estimation-Toolbox [22] for DepthFormer [23]. The only modifications are related to dataset format compatibility. The training setup aligns with the original papers' provided recommendations, only excluding data augmentation to preserve the HD pattern from cropping.

4. Dataset

4.1. Nighttime Synthetic Drive Dataset

Given the absence of public datasets containing HD pattern illumination, we create the Nighttime Synthetic Drive Dataset using Nvidia Drive Sim (Drop 15) simulator [30]. This simulator produces road images with photorealism effort. We adapt simulated vehicles headlights to enable real HD projections based on photometric measurements. Our generated dataset comprises 24,995 images with patterns and 24,995 images with high beam illumination. Examples are displayed in Fig. 3.

We select high beam (HB) as comparison point, considering it to be the maximum normal lighting condition. Moreover, high beam provides more illumination than the checkerboard pattern, ensuring that performance improvement are only due to the pattern contribution. All images are simulated nighttime scenes.

Elements in the scene, such as vehicles, pedestrians, and traffic signs, are randomized in each frame. To account for possible light interference, we simulate other car headlights and randomize ambient light between 0 and 10 lux.

We use five different maps and generate 4,999 frames for both pattern and HB illuminated images in each. Maps are intended to represent major cities in specific regions of the world. Three of them are used for training, one for validation, and one for testing. While the two parts of the dataset are not strictly identical due to randomization of road entities, they share the same maps and randomization code, making the domains comparable.

To approach reality as closely as possible, we account for headlight's optical imperfections using real measured photometry file. Fig. 4 illustrates differences between the ideal control matrix and real projection applied in simulation. Thus, aberrations observed in the pattern, particularly along the edges of the projection, are indicative of these optical imperfections.

All RGB images have a 1920×1080 px resolution and corresponding depth maps. Furthermore, we provide annotations necessary for object detection 2D/3D, normals estimation, semantic and instance segmentation, making the dataset suitable for a multitude of tasks related to autonomous driving.

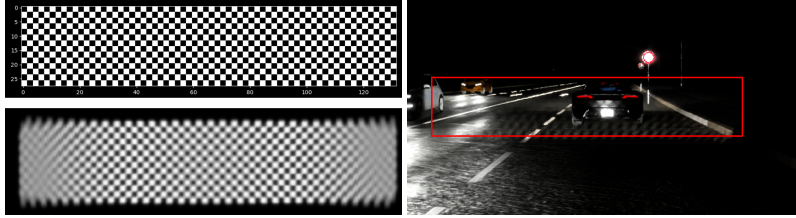


Figure 4. Simulation of HD pattern: The top-left image corresponds to the control matrix of the HD headlight (black=0%, white=100% intensity). At the bottom-left, the generated photometry considering aberrations created by the headlight lens is displayed, particularly noticeable at the edges. On the right, an example of a simulated image using the photometry is presented. The area outlined in red corresponds to the region of interest.

Model	RMSE ↓	Abs Rel ↓	Log ₁₀ ↓	RMSE Log ↓	SILog ↓	Sq Rel ↓	δ^1 ↑	δ^2 ↑	δ^3 ↑
Encoder-decoder (HB)	6.1204	0.0903	0.0233	0.1353	13.4847	3.3579	0.9489	0.9812	0.9908
Encoder-decoder (LED)	5.4259	0.1996	0.0188	0.1253	12.4900	16.1224	0.9603	0.9846	0.9927
Adabins (HB)	7.3520	0.1360	0.0320	0.1230	10.1880	4.2770	0.8790	0.9440	0.9740
Adabins (LED)	5.5830	0.0690	0.0240	0.0920	7.7290	2.5090	0.9210	0.9680	0.9840
DepthFormer (HB)	5.8528	0.0687	0.0281	0.1205	11.3841	0.8328	0.9432	0.9802	0.9913
DepthFormer (LED)	5.3845	0.1215	0.0276	0.1111	10.4146	3.4015	0.9497	0.9838	0.9950

Table 1. Comparison of depth estimation performances: (HB) models are trained on High Beam data and (LED) on HD light pattern. (LED) models outperform (HB) models across all metrics, exceptions are for Abs Rel and Sq Rel. Metrics are computed in the ROI.

As we are not constrained by sensor capabilities, the provided data are not limited, yet we clip the depth at 100 m for all experiments. For reference, KITTI [14] and Oxford RobotCar [27], two real-world road datasets widely used, are respectively limited to 90 m and 50 m. During training, a 640×640 px square is initially center-cropped and then resized to 320×320 px.

To ensure results reproducibility, code and synthetic dataset are publicly available. Releasing large-scale nighttime data, with precise and comprehensive annotations, will foster research on nighttime computer vision for autonomous driving.

4.2. Real-world dataset

We collected an in-house dataset using a real car-mounted prototype to demonstrate the applicability of our method to real-world scenario. It comprises 50,000 images (70% train / 15% val / 15% test) from populated urban and rural roads, evenly split between low beam (LB) illumination and checkerboard pattern with 0.5° , 0.25° and 0.125° cells' dimension. It has been annotated from aggregated and densified LiDAR data using Exwayz software [12]. The HD headlamp we used offers greater projection resolution than the simulated one. More details are available in supplementary materials.

5. Experiments

We evaluate our method through extensive experiments on the Nighttime Synthetic Drive Dataset. We demonstrate

contribution of our light pattern in boosting depth estimation performance, both inside and outside illuminated area. We apply our method to other SOTA approaches: Adabins [4] and DepthFormer [23], showing its extensibility. Finally, we evaluate LED robustness beyond its training domain and its capabilities on real-world scenarios.

The metrics we use in our experiments align with previous works [4, 23, 24, 38, 45, 47]: Root Mean Squared Error (RMSE), Absolute Relative error (Abs Rel), Logarithmic error (Log₁₀), RMSE in Log Space (RMSE Log), Scale-Invariant Logarithmic error (SILog), Squared Relative error (Sq Rel), and threshold accuracy (δ^1 , δ^2 , and δ^3) are employed for a comprehensive evaluation of depth estimation performance.

5.1. HD Pattern Impact

We showcase the depth estimation enhancement obtained by comparing results with and without pattern. As reference we take the encoder-decoder (Sec. 3.1), trained on high beam (HB), while the variant uses our HD pattern (LED). Quantitative and qualitative results are respectively presented in Tab. 1 and Fig. 5.

Quantitative Results. Comparing LED with HB (Tab. 1), we observe a significant improvement in metrics within the ROI: LED yields -11% RMSE. The introduction of the checkerboard pattern leads to a degradation in relative metrics (Abs Rel, Sq Rel). Indeed, when using LED, the model provides a better estimation of distances. However, er-

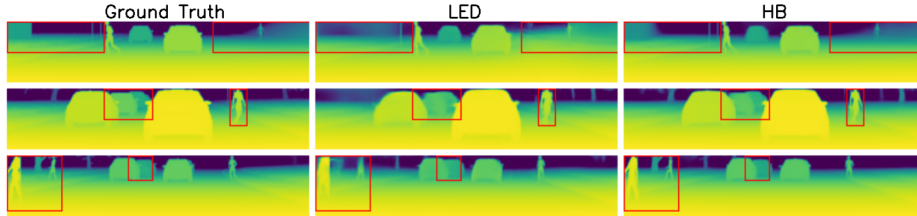


Figure 5. Qualitative results. LED results (right) exhibit higher precision, showcasing more accurate object boundaries and shapes compared to HB (middle). Red boxes indicate enhanced regions.

Model	RMSE ↓	Abs Rel ↓	Log ₁₀ ↓	RMSE Log ↓	SILog ↓	Sq Rel ↓	δ^1 ↑	δ^2 ↑	δ^3 ↑
(HB) O-ROI	9.2533	0.1598	0.0249	0.2047	20.4447	11.4068	0.9385	0.9714	0.9828
(LED) O-ROI	9.0070	0.1295	0.0221	0.2027	20.2348	8.7407	0.9427	0.9723	0.9828
(HB) Full	8.9702	0.1521	0.0247	0.1988	19.8572	10.5225	0.9396	0.9725	0.9836
(LED) Full	8.6963	0.1371	0.0217	0.1965	19.6137	9.5517	0.9446	0.9737	0.9839

Table 2. Encoder-decoder performance beyond ROI: O-ROI stands for Outside ROI, where the evaluation mask is the inverse of the ROI. For Full, metrics calculation is performed on the entire image. (LED) models trained on HD pattern consistently outperform (HB) models in all metrics.

Pattern	RMSE ↓	Abs Rel ↓	SILog ↓
LED	5.497	0.209	12.635
HB	6.443	0.095	13.723
HL	6.668	0.068	14.308
VL	7.360	0.172	15.774

Table 3. Performances using various pattern on half-sized dataset. VL and HL refers to vertical and horizontal lines

rors are often related to pattern occlusions, indiscriminately made on both near and far objects, which impact relative metrics. All metrics assessing the global precision show improvements.

In comparison with the two SOTA approaches [4, 23] mentioned in Tab. 1, LED-trained encoder-decoder either outperforms or matches the performance of their models trained on HB. Considering that the encoder-decoder architecture is inherently less tailored for depth estimation compared to SOTA more intricate designs, this result underscores the substantial improvements yields by LED. Incorporating HD informative pattern, even with straightforward architecture, is therefore promising for challenging nighttime scenarios.

Performance over Distance. Due to the limited visibility at nighttime, depth estimation of distant objects is challenging. In Fig. 6 (a), we showcase the performance of LED over varying distances compared to HB. While maintaining similar performance for close objects (<20m), LED exhibits greater enhancement at longer ranges. Thus, it effectively addresses the task of depth estimation for distant objects at night.

Pattern Study. We generated additional data with various illumination pattern to compare performances between LED checkerboard and other common structured light patterns (horizontal and vertical lines). Tab. 3 demonstrates that choosing the checkerboard pattern leads to the best performance across most metrics. Horizontal lines exhibit slight improvement in relative metrics but a significant decline in other metrics.

ROI-only Training. We investigate whether training the network exclusively on the ROI could potentially enhance our method. This strategy results in an additional improvement of -8.58% Abs Rel, offset by +4.50% RMSE within the specified region, compared to the full-image trained network. This trade-off is valuable for applications where Abs Rel holds greater significance. Additional results can be found in the supplementary material.

5.2. Improving Global Scene Understanding

We investigate the impact of LED on depth estimation beyond ROI. Observed improvement is an indication of the pattern’s contribution to a more holistic scene understanding. Results are presented in Tab. 2.

Performance outside the ROI. Examining depth estimation only outside the ROI, we observe -2.66% improvement in RMSE. We note the absence of degradation in relative metrics, unlike results within the ROI presented in Sec. 5.1. Instead, we report -3.03% Abs Rel and -23.27% Sq Rel. This suggests that the HD headlight pattern provides valuable information for a more accurate understanding of the broader scene geometry. This includes insights into object sizes and scale.

Domain	RMSE ↓	Abs Rel ↓	Log ₁₀ ↓	RMSE Log ↓	SILog ↓	Sq Rel ↓	δ^1 ↑	δ^2 ↑	δ^3 ↑
(HB→HB)	6.1204	0.0903	0.0233	0.1353	13.4847	3.3579	0.9489	0.9812	0.9908
(HB→LED)	17.3113	0.4479	0.1955	0.6817	52.5132	20.0263	0.4699	0.6652	0.7658
(LED→LED)	5.4259	0.1996	0.0188	0.1253	12.4900	16.1224	0.9603	0.9846	0.9927
(LED→HB)	8.0537	0.1511	0.0338	0.2026	20.1120	8.1999	0.9158	0.9626	0.9796

Table 4. Encoder-decoder performance across domains: We denote (training domain → testing domain). The model trained on (HB) fails entirely when tested on (LED). Yet, (LED)-trained models have the ability to estimate depth when tested on the (HB) domain.

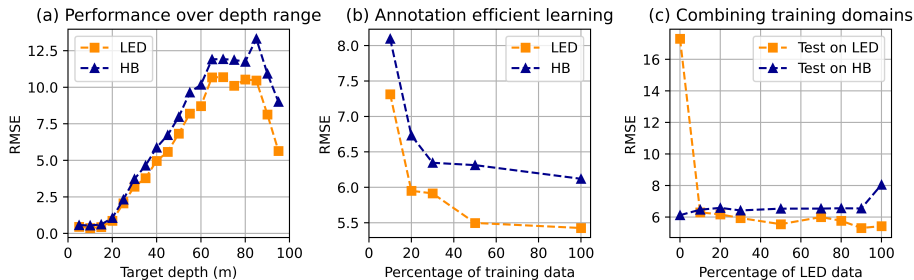


Figure 6. We compare LED to HB in various scenarios. (a) Performance over distance; (b) Performance over training set size; (c) Robustness across domains: Number of training data is fixed and composed of a given ratio of LED and HB data. Overall, LED achieves better long-range results while being more data-efficient. It also demonstrates improved performance across domains.

Performance outside the entire image. Expanding our analysis to the entire image - ROI and outside ROI - we witness improvements such as -3.05% RMSE. Similar to outside ROI, we note -1.50% Abs Rel and -9.23% Sq Rel. This indicates that the HD headlight pattern contributes significantly to the global scene understanding, offering valuable cues that benefit overall depth estimation.

5.3. Annotation-efficient learning

Collecting annotated nighttime data is both challenging and costly, thus, we investigate whether extra guidance provided by the pattern could lead to reduced needs of training data (refer to Fig. 6 (b)). We demonstrate that encoder-decoder trained with less than 20% of the LED data outperforms model trained on the entire HB dataset. Furthermore, model’s performance is near its peak even when trained with only 50% of the dataset.

In addition, we observe that incorporating just 10% of LED data into the HB training set enable the network to learn relevant features and enhance its performances when used with pattern (see Fig. 6 (c)). Therefore, any vehicle equipped with HD headlights can apply LED by adding only a few pattern images in their training set, thereby reducing the cost of specialized data.

5.4. Extensibility to Other SOTA Methods

We extend the evaluation of LED beyond the encoder-decoder architecture, by replicating the methodology of Sec. 5.1 with two additional SOTA architectures. Quantitative results are available in Tab. 1.

As we provide a new annotated dataset, we opt for two

high performing SOTA supervised approaches designed for daytime scenarios: Adabins [4] and DepthFormer [23]. Their use of transformer architectures provides valuable insights into our method behavior when used on more complex architectures.

With the HD pattern, Adabins demonstrates a substantial improvement with -24.06% RMSE and -6.70% Abs Rel within the ROI compared to the HB model. Conversely, DepthFormer showcases -8.00% enhancement in RMSE but +5.28% decrease in Abs Rel. Note that the most significant enhancement is observed in Adabins, which initially had the worst results by night with HB.

Improvements seen across diverse architectures confirm LED agnosticity to architectures. It implies potential effectiveness with future SOTA methods.

5.5. Robustness Across Domains

We evaluate model robustness when operating beyond the original training domain. To this end, we run on HB data the model trained on the pattern and *vice versa*. We report results in Tab. 4.

HB-trained model exhibits a complete failure when confronted to the pattern (+182.85% RMSE). On the contrary, the LED-trained model demonstrates capabilities on HB: although we note +32.63% RMSE, performances are acceptable, with ~ 8 m RMSE (LED→HB) against ~ 17 m (HB→LED).

Furthermore, we demonstrate that incorporating only 10% of HB data is enough to mitigate the performance drop (see Fig. 6 (c)), allowing a unique network to perform well on both domains. In this case, the performance decline is

Model	RMSE ↓	Abs Rel ↓	Log ₁₀ ↓	RMSE Log ↓	SILog ↓	Sq Rel ↓	δ^1 ↑	δ^2 ↑	δ^3 ↑
Encoder-decoder (LB)	14.199	0.187	0.072	0.292	28.938	5.620	0.772	0.909	0.956
Encoder-decoder (LED 0.5°)	11.089	0.119	0.050	0.213	21.251	2.304	0.864	0.950	0.977
Encoder-decoder (LED 0.25°)	8.695	0.109	0.040	0.190	18.635	2.128	0.899	0.963	0.984
Encoder-decoder (LED 0.125°)	10.154	0.096	0.040	0.190	18.862	2.132	0.907	0.969	0.984
DepthFormer (LB)	8.777	0.138	0.050	0.186	17.170	3.365	0.864	0.957	0.983
DepthFormer (LED 0.5°)	6.810	0.101	0.041	0.152	14.380	1.376	0.890	0.969	0.989
DepthFormer (LED 0.25°)	5.621	0.082	0.030	0.126	11.735	1.163	0.923	0.978	0.992
DepthFormer (LED 0.125°)	5.727	0.076	0.030	0.116	10.754	1.261	0.940	0.987	0.995

Table 5. Performance comparison on our real-world dataset using various pattern resolutions: (LED) models outperform (LB) across all metrics, demonstrating LED applicability on real-world scenarios.



Figure 7. Real world qualitative results: DepthFormer LED model produces accurate depth estimation on complex scenes, even in presence of interfering lights, e.g., car headlights, street lights.

reduced to +17.11% RMSE.

This adaptability allows a wider range of applications for the method. It enables selective use of the pattern when higher precision is necessary and its absence when avoiding glare is crucial. The pattern can be applied to specific regions such as objects of interest.

5.6. Real World Scenarios

We show the applicability of our method in real world scenarios using our in-house dataset. We report results in Tab. 5. LED significantly boosts performance over LB, across all metrics. In particular, DepthFormer (0.5°) shows -23.3% RMSE improvement. The qualitative result Fig. 7 shows LED’s robustness under interfering light sources, e.g., car headlights, street lights.

To account for objects passing through the pattern illumination, we investigate the impact of smaller checkerboard cells. Using a size of 0.25°, we observe great enhancement across all metrics (-17.4% RMSE, -18.8% Abs Rel against 0.5°). In contrast, further increasing the checkerboard resolution to 0.125° does not lead to significant improvements. Indeed, pattern features become difficult to distinguish with the camera resolution, thus reducing cues provided to the models. Performances shown by DepthFormer (LED) underpin the benefits of LED in complex real-world scenarios.

6. Limitations and Future Works

While the implicit learning of a reference pattern allows the method to be architecture agnostic, it remains limited to a single pattern defined during training. Moving forward specialized architectures handling the pattern as an integral input element would enable dynamic pattern optimization and improve method generalization.

We demonstrated LED capabilities on different projector-camera distance by training on both real (70 cm) and synthetic (150 cm) setup, meaning that it can be used over a same car model fleet. But it could be sensitive to large discrepancies. We intend to further study the generalization of LED in future works.

It is possible that LED pattern would glare other road users. One way to avoid this would be to leverage HD headlight to mask road users [39]. Safety issues and the impact of selective illumination on performance should be assessed in future works.

7. Conclusion

We introduce LED, a novel method for enhancing nighttime depth estimation, leveraging HD light patterns projected by modern vehicle headlights. Through extensive experiments, we demonstrate the effectiveness of our approach, showcasing notable improvements in depth perception within and beyond illuminated areas. The versatility of our method is further emphasized by its successful integration with two SOTA architectures: Adabins and DepthFormer. Moreover, LED demonstrated promising real-world performances. We release the Nighttime Synthetic Drive Dataset, a synthetic nighttime dataset comprising 49,995 comprehensively annotated images. This dataset will serve as a valuable resource for the research community, fostering exploration of various tasks related to autonomous driving in low-light conditions. As we tackle the difficulties of nighttime computer vision, our study highlights the potential advantages of using HD patterns for robust depth estimation.

Acknowledgments

We would like to thank Amandine Brunetto for her help and insights.

References

- [1] Ashutosh Agarwal and Chetan Arora. Attention attention everywhere: Monocular depth prediction with skip attention. In *WACV*, 2023. 1, 2
- [2] Seung-Hwan Baek and Felix Heide. Polka Lines: Learning Structured Illumination and Reconstruction for Active Stereo. In *CVPR*, 2021. 1, 2
- [3] Nicholas Baker, Hongjing Lu, Gennady Erlikhman, and Philip J Kellman. Local features and global shape information in object classification by deep convolutional neural networks. *VR*, 2020. 3
- [4] Shariq Farooq Bhat, Ibraheem Alhashim, and Peter Wonka. Adabins: Depth estimation using adaptive bins. In *CVPR*, 2021. 1, 2, 3, 4, 5, 6, 7, 11
- [5] Jiawang Bian, Zhichao Li, Naiyan Wang, Huangying Zhan, Chunhua Shen, Ming-Ming Cheng, and Ian Reid. Unsupervised scale-consistent depth and ego-motion learning from monocular video. In *NeurIPS*, 2019. 1, 2
- [6] Mario Bijelic, Tobias Gruber, and Werner Ritter. A benchmark for lidar sensors in fog: Is detection breaking down? In *IV*, 2018. 1
- [7] Mario Bijelic, Tobias Gruber, and Werner Ritter. Benchmarking image sensors under adverse weather conditions for autonomous driving. In *IV*, 2018. 1
- [8] Gayan Brahmanage and Henry Leung. Outdoor RGB-D Mapping Using Intel-RealSense. In *IEEE Sensors*, 2019. 2
- [9] Holger Caesar, Varun Bankiti, Alex H. Lang, Sourabh Vora, Venice Erin Liong, Qiang Xu, Anush Krishnan, Yu Pan, Giancarlo Baldan, and Oscar Beijbom. nuscenes: A multi-modal dataset for autonomous driving. In *CVPR*, 2020. 2
- [10] Bowen Cheng, Ishan Misra, Alexander G. Schwing, Alexander Kirillov, and Rohit Girdhar. Masked-attention mask transformer for universal image segmentation. *arXiv*, 2021. 13, 14
- [11] Raul De Charette, Robert Tamburo, Peter C. Barnum, Anthony Rowe, Takeo Kanade, and Srinivasa G. Narasimhan. Fast reactive control for illumination through rain and snow. In *ICCP*, 2012. 2
- [12] Exwayz. Exwayz 3d mapping: Create dense, accurate and georeferenced 3d point cloud using lidar slam. <https://www.exwayz.fr/>, 2024. 5, 14
- [13] Sean Ryan Fanello, Christoph Rhemann, Vladimir Tankovich, Adarsh Kowdle, Sergio Orts Escolano, David Kim, and Shahram Izadi. HyperDepth: Learning Depth from Structured Light without Matching. In *CVPR*, 2016. 1, 2
- [14] Andreas Geiger, Philip Lenz, and Raquel Urtasun. Are we ready for autonomous driving? the kitti vision benchmark suite. In *CVPR*, 2012. 2, 5
- [15] Clément Godard, Oisín Mac Aodha, and Gabriel J Brostow. Unsupervised monocular depth estimation with left-right consistency. In *CVPR*, 2017. 1
- [16] Clément Godard, Oisín Mac Aodha, Michael Firman, and Gabriel J Brostow. Digging into self-supervised monocular depth estimation. In *ICCV*, 2019. 1, 2
- [17] Vitor Guizilini, Rares Ambrus, Sudeep Pillai, Allan Raventos, and Adrien Gaidon. 3d packing for self-supervised monocular depth estimation. In *CVPR*, 2020. 1, 2
- [18] Mohit Gupta, Qi Yin, and Shree K. Nayar. Structured Light in Sunlight. In *ICCV*, 2013. 2
- [19] Junjie Hu, Mete Ozay, Yan Zhang, and Takayuki Okatani. Revisiting single image depth estimation: Toward higher resolution maps with accurate object boundaries. In *WACV*, 2019. 3, 4
- [20] Jin Han Lee, Myung-Kyu Han, Dong Wook Ko, and Il Hong Suh. From big to small: Multi-scale local planar guidance for monocular depth estimation. *arXiv preprint arXiv:1907.10326*, 2019. 1, 2
- [21] Chunyu Li, Yusuke Monno, and Masatoshi Okutomi. Deep Hyperspectral-Depth Reconstruction Using Single Color-Dot Projection. In *CVPR*, 2022. 1, 2
- [22] Zhenyu Li. Monocular depth estimation toolbox. <https://github.com/zhyever/Monocular-Depth-Estimation-Toolbox>, 2022. 4
- [23] Zhenyu Li, Zehui Chen, Xianming Liu, and Junjun Jiang. Depthformer: Exploiting long-range correlation and local information for accurate monocular depth estimation. *MIR*, 2023. 1, 2, 3, 4, 5, 6, 7, 11
- [24] Lina Liu, Xibin Song, Mengmeng Wang, Yong Liu, and Liangjun Zhang. Self-supervised monocular depth estimation for all day images using domain separation. In *ICCV*, 2021. 1, 2, 5
- [25] Ilya Loshchilov and Frank Hutter. Decoupled weight decay regularization. In *ICLR*, 2018. 4
- [26] Yawen Lu and Guoyu Lu. An alternative of lidar in nighttime: Unsupervised depth estimation based on single thermal image. In *WACV*, 2021. 2
- [27] Will Maddern, Geoff Pascoe, Chris Linegar, and Paul Newman. 1 Year, 1000km: The Oxford RobotCar Dataset. *IJRR*, 2017. 2, 5
- [28] Christoph Mertz, Sanjeev J. Koppal, Solomon Sia, and Srinivasa Narasimhan. A low-power structured light sensor for outdoor scene reconstruction and dominant material identification. In *CVPR Workshops*, 2012. 2
- [29] Pushmeet Kohli, Nathan Silberman, Derek Hoiem and Rob Fergus. Indoor segmentation and support inference from rgb-d images. In *ECCV*, 2012. 2
- [30] NVIDIA. Nvidia drive sim. <https://www.nvidia.com/en-us/self-driving-cars/simulation/>. Accessed: 2024-01-18. 4
- [31] Adam Paszke, Sam Gross, Francisco Massa, Adam Lerer, James Bradbury, Gregory Chanan, Trevor Killeen, Zeming Lin, Natalia Gimelshein, Luca Antiga, Alban Desmaison, Andreas Kopf, Edward Yang, Zachary DeVito, Martin Raison, Alykhan Tejani, Sasank Chilamkurthy, Benoit Steiner, Lu Fang, Junjie Bai, and Soumith Chintala. Pytorch: An imperative style, high-performance deep learning library. In *NeurIPS*, 2019. 4

- [32] Matteo Poggi, Filippo Aleotti, Fabio Tosi, and Stefano Mattoccia. Towards real-time unsupervised monocular depth estimation on cpu. In *IROS*, pages 5848–5854. IEEE, 2018. [1](#), [2](#)
- [33] Gernot Riegler, Yiyi Liao, Simon Donne, Vladlen Koltun, and Andreas Geiger. Connecting the Dots: Learning Representations for Active Monocular Depth Estimation. In *CVPR*, 2019. [1](#), [2](#)
- [34] Olaf Ronneberger, Philipp Fischer, and Thomas Brox. U-net: Convolutional networks for biomedical image segmentation. In *MICCAI*, 2015. [3](#), [11](#)
- [35] Ukcheol Shin, Jinsun Park, and In So Kweon. Deep depth estimation from thermal image. In *CVPR*, 2023. [2](#)
- [36] Chang Shu, Kun Yu, Zhixiang Duan, and Kuiyuan Yang. Feature-metric loss for self-supervised learning of depth and egomotion. In *ECCV*, 2020. [1](#), [2](#)
- [37] Nathan Silberman and Rob Fergus. Indoor scene segmentation using a structured light sensor. In *ICCV Workshops*, 2011. [1](#)
- [38] Jaime Spencer, Richard Bowden, and Simon Hadfield. Defeat-net: General monocular depth via simultaneous unsupervised representation learning. In *CVPR*, 2020. [1](#), [2](#), [5](#)
- [39] Robert Tamburo, Eriko Nurvitadhi, Abhishek Chugh, Mei Chen, Anthony Rowe, Takeo Kanade, and Srinivasa G. Narasimhan. Programmable Automotive Headlights. In *ECCV*, 2014. [2](#), [8](#)
- [40] Madhu Vankadari, Sourav Garg, Anima Majumder, Swagat Kumar, and Ardhendu Behera. Unsupervised monocular depth estimation for night-time images using adversarial domain feature adaptation. In *ECCV*, 2020. [1](#), [2](#)
- [41] Mirko Waldner and Torsten Bertram. Optimal Real-time Digitization of Matrix-Headlights. In *AIM*, 2021. [1](#), [3](#)
- [42] Mirko Waldner, Maximilian Kramer, and Torsten Bertram. Hardware-in-the-Loop-Simulation of the light distribution of automotive Matrix-LED-Headlights. In *AIM*, 2019. [1](#), [3](#)
- [43] Mirko Waldner, Maximilian Kramer, and Torsten Bertram. Digitization of Matrix-Headlights That Move as in the Real Test Drive. In *AIM*, 2020. [1](#), [3](#)
- [44] Mirko Waldner, Nathalie Müller, and Torsten Bertram. Energy-Efficient Illumination by Matrix Headlamps for Nighttime Automated Object Detection. *IJECER*, 2022. [3](#)
- [45] Kun Wang, Zhenyu Zhang, Zhiqiang Yan, Xiang Li, Baobei Xu, Jun Li, and Jian Yang. Regularizing nighttime weirdness: Efficient self-supervised monocular depth estimation in the dark. In *CVPR*, 2021. [1](#), [2](#), [5](#)
- [46] Zhichao Yin and Jianping Shi. Geonet: Unsupervised learning of dense depth, optical flow and camera pose. In *CVPR*, 2018. [1](#), [2](#)
- [47] Yupeng Zheng, Chengliang Zhong, Pengfei Li, Huan-ang Gao, Yuhang Zheng, Bu Jin, Ling Wang, Hao Zhao, Guyue Zhou, Qichao Zhang, et al. Steps: Joint self-supervised nighttime image enhancement and depth estimation. In *ICRA*, 2023. [1](#), [2](#), [5](#)
- [48] Tinghui Zhou, Matthew Brown, Noah Snavely, and David G Lowe. Unsupervised learning of depth and ego-motion from video. In *CVPR*, 2017. [1](#), [2](#)

Supplementary Material

A. ROI Definition

To assess the impact of the LED pattern, we define a Region of Interest (ROI) representing the illuminated area in most images and calculate our metrics within this region. We center-crop the image to 640×640 px and then resize it to 320×320 px. In the resulting image, the ROI consists of pixels with coordinates satisfying: $20 \leq p_x \leq 270$ and $165 \leq p_y \leq 210$, where p_x and p_y are the pixel coordinates along the x and y axes, respectively.

B. ROI-Only Training

To assess our method’s impact, we focus on the illuminated area. Thus, it is reasonable to evaluate performance when trained exclusively within the ROI. We report results of this experiment in Tab. S1. We observe that training solely within the ROI enhances Abs Rel and Sq Rel metrics, although other metrics show a decline. Since the network’s ability to estimate depth beyond the ROI is valuable for many applications, we opt not to pursue this approach.

Image input	RMSE ↓	Abs Rel ↓	Log ₁₀ ↓	RMSE Log ↓	SILog ↓	Sq Rel ↓	δ^1 ↑	δ^2 ↑	δ^3 ↑
Reference	5.4259	0.1996	0.0188	0.1253	12.4900	16.1224	0.9603	0.9846	0.9927
ROI-Only	5.6931	0.1145	0.0199	0.1428	14.2131	4.4541	0.9585	0.9841	0.9932

Table S1. Comparison of encoder-decoder performances between ROI-only training and baseline.

C. Resolution Impact

Resolution and performance are usually highly correlated in computer vision, particularly in low-light conditions. To better understand the impact of resolution on our method, we train the encoder-decoder with center-cropped area resized at various resolutions. Results in Tab. S2 indicate that increasing resolution up to 640×640 px does not improve performance. Conversely, decreasing resolution to 200×200 px appears to enhance relative metrics while degrading others. Since most valuable cues in our method come from the pattern, these findings suggest that a resolution of 320×320 px offers a favorable trade-off for pattern visibility and scene interpretation within our setup (as shown in Fig. S1).

Resolution	RMSE ↓	Abs Rel ↓	Log ₁₀ ↓	RMSE Log ↓	SILog ↓	Sq Rel ↓	δ^1 ↑	δ^2 ↑	δ^3 ↑
200 px	5.9413	0.1073	0.0206	0.1270	12.6227	3.9736	0.9545	0.9228	0.9921
320 px	5.4259	0.1996	0.0188	0.1253	12.4900	16.1224	0.9603	0.9846	0.9927
640 px	5.7050	0.2109	0.0185	0.1420	14.1092	17.4085	0.9668	0.9837	0.9893

Table S2. Encoder-decoder performances at various resolutions.

D. Encoder-Decoder Details

LED uses a single pattern implicitly learned by the model, making it architecture-agnostic. This characteristic is demonstrated in the main paper (see Sec. 5.4) by applying LED to multiple state-of-the-art architectures [4, 23]. To prove our concept and conduct experiments, we opt for an encoder-decoder architecture with skip connections [34]. The detailed architecture is shown in Fig. S2. Despite the simplicity of this architecture, we show that LED enables the network to achieve performances comparable to or better than other tested SOTA architectures trained without our method.

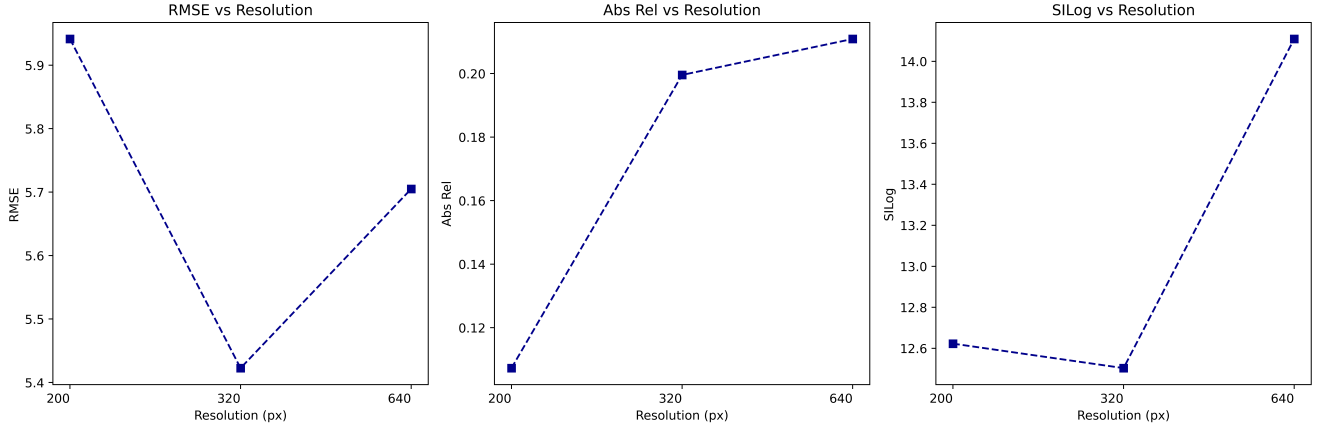


Figure S1. Performances using multiple resolutions

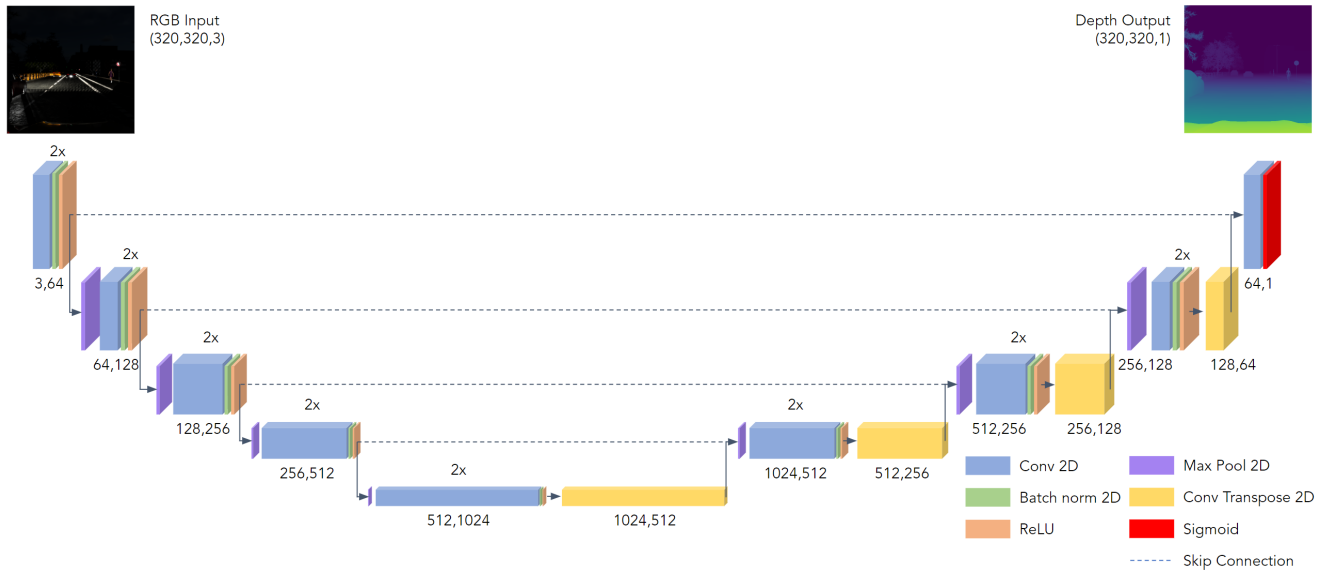


Figure S2. Detailed encoder-decoder architecture

E. Loss Study

To determine the impact of each individual loss, we conduct an ablation study (see Tab. S3). Both L1 and Log L1 losses are tested for \mathcal{L}_{depth} and \mathcal{L}_{grad} . Our findings indicate that each selected loss positively influences performance. The combination outlined in the paper (Sec. 3.3) demonstrates the most favorable trade-off between metrics.

F. Examples of Other Patterns

To find a suitable pattern for our application, we generate half-sized datasets featuring commonly used structured light patterns: checkerboard, horizontal, and vertical lines (see Fig. S3). Comprehensive metrics from this experiment are available in Tab. S4, the checkerboard pattern demonstrates significantly superior performances.

\mathcal{L}_{depth}		\mathcal{L}_{grad}		\mathcal{L}_{normal}	Metrics								
L1	Log L1	L1	Log L1		RMSE ↓	Abs Rel ↓	Log ₁₀ ↓	RMSE Log ↓	SILog ↓	Sq Rel ↓	$\delta^1 \uparrow$	$\delta^2 \uparrow$	$\delta^3 \uparrow$
✓	✗	✗	✗	✗	5.979	0.191	0.020	0.132	13.032	14.352	0.957	0.982	0.991
✗	✓	✗	✗	✗	5.852	0.187	0.021	0.132	13.122	12.984	0.957	0.983	0.992
✗	✓	✓	✗	✗	5.760	0.201	0.020	0.137	13.616	16.174	0.958	0.983	0.992
✗	✓	✗	✓	✗	5.386	0.202	0.021	0.124	12.373	15.901	0.958	0.985	0.993
✗	✓	✗	✗	✓	5.309	0.206	0.022	0.149	14.862	16.048	0.954	0.981	0.990
✗	✓	✗	✓	✓	5.809	0.186	0.018	0.125	12.210	14.683	0.961	0.985	0.993
✗	✓	✓	✗	✓	5.422	0.200	0.018	0.125	12.503	16.120	0.961	0.985	0.993

Table S3. Performance comparison using several combination of losses: **1st best**, 2nd best, 3rd best.



Figure S3. Example of tested illuminations: high-beam (top-left), checkerboard (top-right), horizontal lines (bottom-left) and vertical lines (bottom-right)

G. LED Impact On Other Tasks

LED lighting pattern is mostly suitable for geometric tasks. We study its impact on other tasks performances, taking the example of semantic segmentation. To this end, we trained Mask2Former [10] using the available annotation in the Nighttime Synthetic Drive Dataset. Results are reported in Tab. S5. LED doesn't improve, nor degrade performances. We even note a better stability with less variance over runs. Therefore, the similar performance on both domains suggests that LED enhances geometric tasks with limited impact on semantic ones.

H. Real World Scenarios

To collect our real-world dataset, we made a prototype on a real car. We used an IDS U3-36L0XC camera and an Ouster OS1-128 LiDAR (Rev 7). Regarding the HD headlight, we opt for the Digital Micromirror Device technology, which offer the

Pattern	RMSE ↓	Abs Rel ↓	Log ₁₀ ↓	RMSE Log ↓	SILog ↓	Sq Rel ↓	δ^1 ↑	δ^2 ↑	δ^3 ↑
LED	5.5179	0.1977	0.0196	0.1233	12.2798	15.6867	0.9593	0.9849	0.9931
HB	6.0937	0.0867	0.0216	0.1298	12.8895	3.1352	0.9521	0.9824	0.9917
VL	7.3598	0.1723	0.0264	0.1600	15.7743	6.5203	0.9393	0.9751	0.9876
HL	6.6679	0.0681	0.0254	0.1445	14.3077	1.2319	0.9370	0.9776	0.9903

Table S4. Comparison of encoder-decoder performances using various patterns: LED use the checkerboard, HB stands for high-beam, VL and HL are vertical and horizontal lines respectively.

Model	mIoU ↑
Mask2Former (LB)	51.45 ± 4,00
Mask2Former (LED)	51.49 ± 0,76

Table S5. Semantic segmentation results on the Nighttime Synthetic Drive Dataset using Mask2Former [10]

greatest resolution ($<0.015^\circ$) with a horizontal FOV of 14° and vertical FOV of 7° . All the hardware was mounted on the roof of the car. This novel setup allowed us to test LED under another projector-camera configuration. Ground truth annotation was made using LiDAR data, aggregated and densified thanks to Exwayz software [12]. Due to the high resolution of the headlight we were able to collect data with smaller cell size than in simulation, giving more insight into pattern resolution impact. Model’s performances on the dataset demonstrate LED capabilities on complex real-world scenarios. We showcase more qualitative results in Fig. S4. A video of Depthformer (LED 0.25°) qualitative results on our real-world dataset is available in the supplementary material.

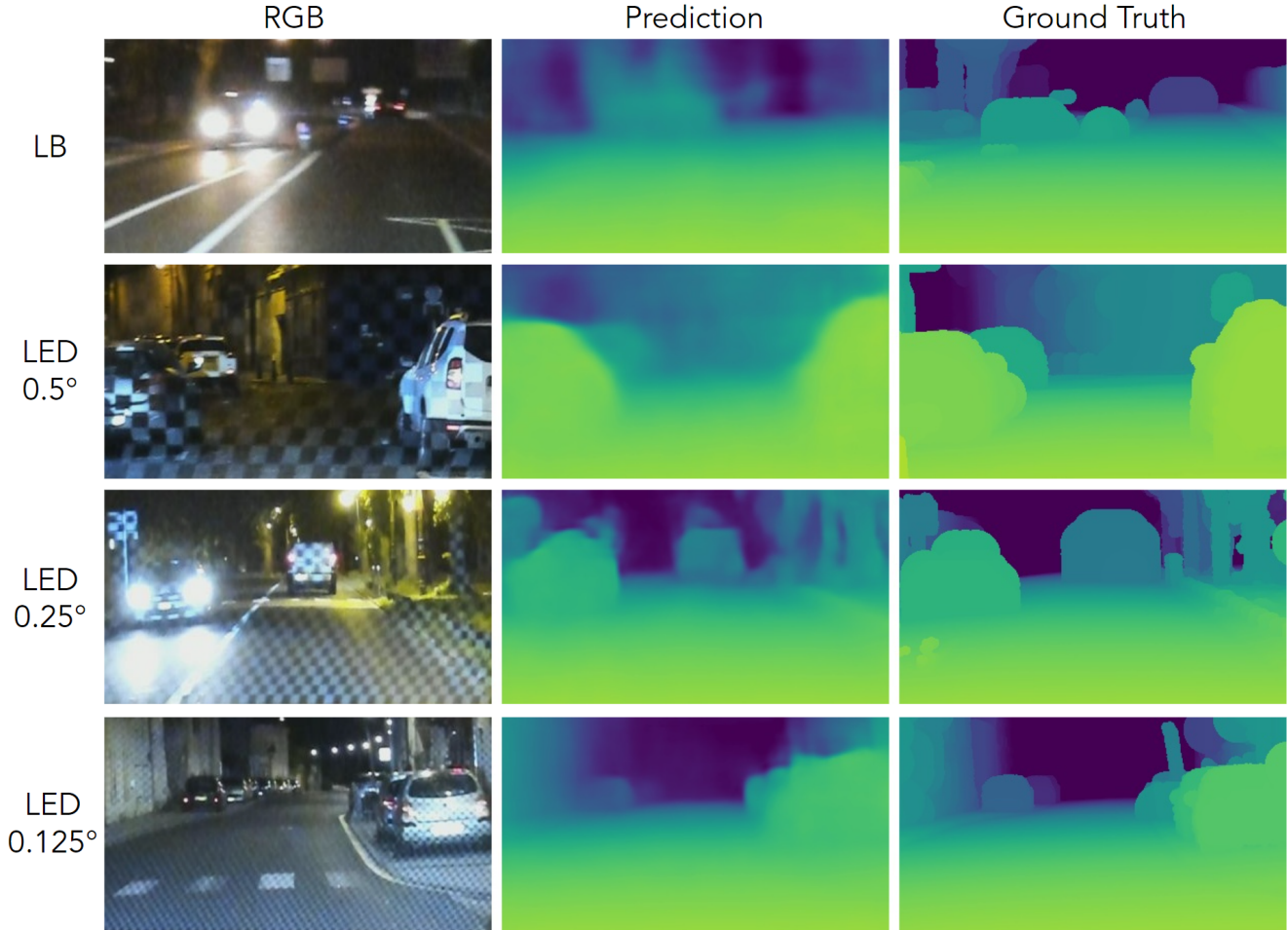


Figure S4. Qualitative results on real-world scenarios. LED-trained models are more accurate and object edges are better defined.

I. Multiple Resolutions Robustness

Any HD headlight can project LED’s checkerboard, although with a resolution adjustment. To evaluate its impact on model performances, we propose to train a model with 3 checkerboard resolutions (0.5° , 0.25° and 0.125°) evenly split, and evaluate on each one. Table S6 demonstrates that the model is able to perform well on all resolutions although with a minor performance degradation compared to single resolution training. This shows our model’s ability to generalize over multiple resolutions, thus, various HD headlights or car models.

Test set	RMSE ↓	Abs Rel ↓	Log ₁₀ ↓	RMSE Log ↓	SILog ↓	Sq Rel ↓	δ^1 ↑	δ^2 ↑	δ^3 ↑
LED (0.5°)	6.859	0.102	0.041	0.153	14.162	1.511	0.894	0.971	0.989
LED (0.25°)	5.787	0.082	0.033	0.126	11.875	1.0839	0.929	0.983	0.994
LED (0.125°)	5.730	0.077	0.030	0.116	10.913	1.149	0.958	0.989	0.995

Table S6. DepthFormer results when trained on 33% of each checkerboard resolutions (0.5° , 0.25° , 0.125°).

J. Qualitative Results on Synthetic Dataset

We showcase the depth estimation enhancement obtained by comparing results with and without pattern. They are obtained by taking the encoder-decoder, trained on high beam (HB), and with our HD pattern (LED). Red boxes emphasize on enhanced regions. Some are zoomed in for improved visibility. LED results (right) exhibit higher precision, showcasing more accurate object boundaries and shapes compared to HB (middle). Far away obstacles are better defined and less blurry (first row), vehicles and pedestrians are sharper (second rows).

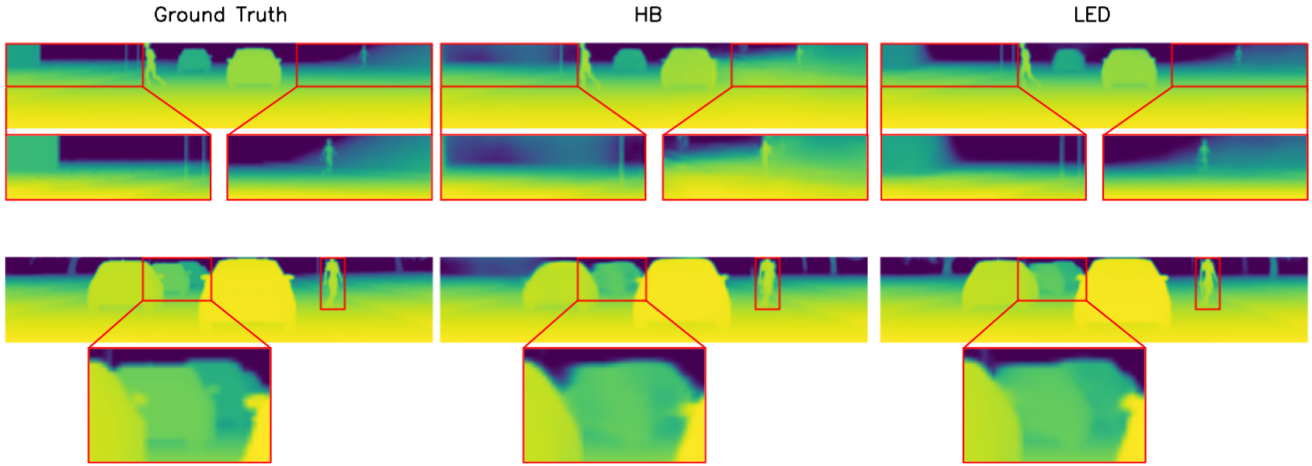


Figure S5. Zoomed in qualitative results showcasing LED improved depth prediction compared to high-beam (HB).

K. Safety and Regulation

While using readily available hardware, LED is a research project not meant to be deployed on cars right away. Future works should assess potential safety issues. To maximize their safety, autonomous vehicles needs multiple perception mechanisms that ensure redundancy, compensating for blind spots of other sensors on the car, *e.g.*, LiDAR in rain conditions. One can imagine that this feature could be turned off in crowded areas, or when detecting an incoming car after it was initially detected at a longer distance, ensuring safety. Regarding regulation, HD headlight technology is novel and the European regulation has authorized just recently the projection of specific HD pattern onto the road. Thus, laws are moving in this direction and evolving with the technology.